www.nature.com/cdd

CDDpress

ARTICLE

NAT10 regulates mitotic cell fate by acetylating Eg5 to control bipolar spindle assembly and chromosome segregation

Jiaojiao Zheng[1,4], Yuqin Tan[1,4], Xiaofeng Liu[2], Chunfeng Zhang[3], Kunqi Su[1], Yang Jiang[1], Jianyuan Luo[3], Li Li[1]✉ and Xiaojuan Du[1]✉

Cell fate of mitotic cell is controlled by spindle assembly. Deficient spindle assembly results in mitotic catastrophe leading to cell death to maintain cellular homeostasis. Therefore, inducing mitotic catastrophe provides a strategy for tumor therapy. Nucleolar acetyltransferase NAT10 has been found to regulate various cellular processes to maintain cell homeostasis. Here we report that NAT10 regulates mitotic cell fate by acetylating Eg5. NAT10 depletion results in multinuclear giant cells, which is the hallmark of mitotic catastrophe. Live-cell imaging showed that knockdown of NAT10 dramatically prolongs the mitotic time and induces defective chromosome segregation including chromosome misalignment, bridge and lagging. NAT10 binds and co-localizes with Eg5 in the centrosome during mitosis. Depletion of NAT10 reduces the centrosome loading of Eg5 and impairs the poleward movement of centrosome, leading to monopolar and asymmetrical spindle formation. Furthermore, NAT10 stabilizes Eg5 through its acetyltransferase function. NAT10 acetylates Eg5 at K771 to control Eg5 stabilization. We generated K771-Ac specific antibody and showed that Eg5 K771-Ac specifically localizes in the centrosome during mitosis. Additionally, K771 acetylation is required for the motor function of Eg5. The hyper-acetylation mimic Flag-Eg5 K771Q but not Flag-Eg5 rescued the NAT10 depletion-induced defective spindle formation and mitotic catastrophe, demonstrating that NAT10 controls mitosis through acetylating Eg5 K771. Collectively, we identify Eg5 as an important substrate of NAT10 in the control of mitosis and provide K771 as an essential acetylation site in the stabilization and motor function of Eg5. Our findings reveal that targeting the NAT10-mediated Eg5 K771 acetylation provides a potential strategy for tumor therapy.

Cell Death & Differentiation (2022) 29:846–860; https://doi.org/10.1038/s41418-021-00899-5

INTRODUCTION

Faithful segregation of chromosomes into the nascent daughter cells is critical for maintaining genomic integrity [1, 2]. Errors in karyokinesis and/or cytokinesis during cell division generate abnormal genomic content including aneuploidy or polyploidy [3]. When these errors cannot be corrected, they ultimately lead to mitotic catastrophe, a key mechanism that prevents the proliferation and survival of mitotically aberrant cells through cell death and senescence [3, 4]. Disrupting mitotic catastrophe process causes persistent genomic instability, a well-characterized hallmark of cancer [5]. Therefore, mitotic catastrophe is a critical mechanism to prevent cells from becoming tumorigenic and its induction constitutes a therapeutic endpoint [3].

Perturbations of mitotic spindle function often induce mitotic catastrophe [6]. The mitotic spindle microtubules (MTs) interact with motor proteins to generate spindle-stabilizing tensions and chromosome-moving forces during mitosis [7]. The motor protein Eg5, a Kinesin-5 family member, is essential for spindle bipolarity [8, 9]. The Eg5 inhibitors including Monastrol, K858 and ARRY-520 trigger mitotic catastrophe and cell death [10–12]. ARRY-520, alone or in combination with other anticancer agents, is currently under clinical trials for the treatment of malignant tumor [13, 14]. Therefore, identification of Eg5 regulators will provide more choices for cancer therapy.

The localization and function of Eg5 has been found to be controlled by the post-translational modifications (PTMs) [15]. Phosphorylation of Eg5 at various sites is required for its spindle localization and motor function [15–17]. The acetylation at K146 in the motor domain of Eg5 enhances the binding of Eg5 with MTs and attenuates the dissociation from MTs to slow the poleward movement, thus acting as a "brake" of mitosis [18, 19]. Acetylation at K890 inhibits the ATP hydrolysis capability of Eg5 and blocks spindle assembly, while deacetylation of K890 by HDAC promotes mitosis [20]. Therefore, identification of Eg5 PTMs will help us to better understand the mitosis control.

Since Eg5 function determines the cell fate of mitotic cells, its expression must be tightly controlled. It is reported that Eg5 is protected from degradation by the RNF20/40 complex through promoting the mono-ubiquitination at K745 during mitosis [21]. Additionally, expression level of Eg5 is reduced by the anaphase-

[1]Department of Cell Biology, School of Basic Medical Sciences, Peking University Health Science Center, 100191 Beijing, China. [2]Hepatopancreatobiliary Surgery Department I, Key Laboratory of Carcinogenesis and Translational Research (Ministry of Education), Peking University School of Oncology, Beijing Cancer Hospital & Institute, 100142 Beijing, China. [3]Department of Medical Genetics, School of Basic Medical Sciences, Peking University Health Science Center, 100191 Beijing, China. [4]These authors contributed equally: Jiaojiao Zheng, Yuqin Tan. ✉email: lily@bjmu.edu.cn; duxiaojuan100@bjmu.edu.cn

Edited by H Ichijo

Received: 9 April 2021 Revised: 7 November 2021 Accepted: 9 November 2021
Published online: 24 February 2022

promoting complex/cyclosome (APC/C)-mediated ubiquitin-proteasome pathway in the cancer cells with centrosome amplifications [22]. Therefore, the PTMs of Eg5 play essential roles in the control of its expression level.

The nucleolar N-acetyltransferase 10 (NAT10, also named hALP) participates in multiple cellular biological processes via its acetyltransferase activity. In the nucleolus, NAT10 participates in the rRNA biogenesis by acetylating UBF (upstream binding factor) and rRNA [23–25]. NAT10 also acetylates cytosine of tRNA [26], and promotes mRNA stability and translation efficiency by acetylating cytidine of mRNA [27–29]. Importantly, NAT10 maintains cellular homeostasis under stress conditions by acetylating key checkpoint proteins. For instance, NAT10 acetylates p53, PARP1 and MORC2 upon DNA damage to avoid proliferation of genomic damaged cell [30–32]. Under energy stress, NAT10 controls the transition from rRNA biogenesis to autophagy through regulating Che-1 acetylation to support cell survival [33]. Thus, NAT10 plays multiple roles in various biological and pathological processes by catalyzing specific substrates.

Recently, it has been found that the dysregulation of NAT10 is associated with human diseases. A specific NAT10 inhibitor Remodelin has been found to be a potential remedy for the Hutchinson-Gilford progeria syndrome (HGPS) [34]. In addition, NAT10 dysregulation is correlated with various types of cancers including colorectal cancer (CRC), hepatocellular carcinoma (HCC), melanoma and breast cancer [32, 34–41]. Thus, targeting NAT10 will provide a promising strategy for disease intervention and tumor treatment.

At the onset of mitosis, nuclear envelope breaks down, interphase chromatin condenses into mitotic chromosomes, nucleolus disappears, the ribosome biogenesis ceases and the nucleolar proteins either disperse in the cells, spread around or between chromosomes, or is destroyed [42–44]. However, the function of nucleolar proteins in mitosis is not fully understood. NAT10 has been found to be involved in the chromosome de-condensation, nucleolar assembly and cytokinesis at the end of mitosis [45, 46]. However, how NAT10 regulates mitosis remains unclear.

In the present study, we found that NAT10 depletion leads to mitotic catastrophe by inducing disorder of spindle assembly and defective chromosome segregation during mitosis. NAT10 binds Eg5 at centrosome and stabilizes Eg5 through acetylation. NAT10 acetylates Eg5 at K771, and Eg5 K771-Ac specifically localizes at the centrosome in mitosis. Furthermore, K771-Ac is required for the motor function of Eg5. The hyper-acetylation mimic Flag-Eg5 K771Q, but not Flag-Eg5 or Flag-Eg5 K771R, rescues the NAT10 deficiency-induced defective spindle formation and mitotic catastrophe. Thus, targeting the NAT10-mediated Eg5 acetylation at K771 provides a promising strategy for tumor treatment.

MATERIAL AND METHODS

Cell culture and transfection

H1299, HeLa, HCT116 and HEK 293 cells were maintained in DMEM supplemented with 10% fetal bovine serum. These cell lines were purchased from cell bank of Chinese Academy of Medical Sciences. Cells were routinely tested for Mycoplasma contamination. Cells were transfected with plasmid DNA or siRNA duplexes using Lipofectamine 2000 (Invitrogen) according to the manufacturer's protocol. In transient transfection experiments, plasmid DNA concentrations were maintained at a constant level with an empty vector.

CRISPR-Cas9-mediated genome editing

The HeLa Ctrl and HeLa *NAT10* knockout (KO) cell lines were established by CRISPR–Cas9 genome editing technology in our laboratory. Briefly, HeLa cells were co-transfected with Topo-Cas9-IRES-EGFP and pc3-U6-NAT10-g1-CMV-Red. Twenty-four hours later, the double-positive cells (green & red) were sorted by flow cytometry and cultured for 3 days. Then, single cells were seeded into 96-well plates. Mutation of *NAT10* gene was verified by DNA sequencing and the NAT10 protein level was evaluated by Western blot in the independent mono-clone cells. The HeLa-*NAT10* KO cell lines were maintained in DMEM medium, supplemented with 10% serum. Genomic DNA was extracted from the HeLa *NAT10* KO cell lines C4 and C19, and *NAT10* gene was amplified by PCR. The amplified *NAT10* fragments from C4 or C19 cells were sub-cloned into p-GEM-T vector and the sub-clones were subjected to DNA sequencing (RuiBiotech, Beijing, China). For editing *NAT10* gene, the sgRNAs, #1 ACATGCCGAAGG-TATTGCCC and #2 CAACGAGACCCACAAGATCC were used as described previously [30].

Plasmids and antibodies

Flag-NAT10, Flag-NAT10 G641E, Flag-NAT10 K426R, GST-NAT10 and its deletion mutant plasmids were generated in our laboratory [33]. Flag- or GFP-tagged Eg5 and Eg5 mutants were cloned into the pCI-neo or pEGFP-C2 vector. GFP-tagged RNF20 and RNF40 plasmids were gifts from Prof. Xuan lab [21]. GST-Eg5, GST-Eg5 deletion mutants and GST-NAT10 deletion mutants were cloned into the pGEX-4T1 vector. His-Eg5 were cloned into pET-28b(+) vector. For generating stable cell line, GFP-Flag-tagged Eg5 and its mutants were cloned into pLV-hef1a-mNeongreen-WPRE-CMV-MCS. All plasmids cloned with PCR inserts were confirmed by DNA sequencing. Eg5 mutant plasmids including pCI-neo-Flag-Eg5-K771R, pCI-neo-Flag-K771Q, pLV-hef1a-mNeongreen-WPRE-CMV-MCS-Eg5-K771R-3×Flag, pLV-hef1a-mNeongreen-WPRE-CMV-MCS-Eg5-K771R-3×Flag, pGEX-4T1-Eg5-K771R were obtained by mutagenesis using the QuickChange Site-Directed Mutagenesis Kit (Stratagene) according to the manufacturer's protocol. The presence of mutations in the constructed plasmids were confirmed by DNA sequencing.

Anti-Eg5 (ab51976 1:1000), anti-α-tubulin (EP1332Y, 1:1000), anti-γ-tubulin (EPR16793, 1:1000) and anti-α-tubulin (DM1A, 1:20000) were purchased from Abcam. Anti-actin was purchased from ABclonal. Anti-Flag (F3165, 1:1000), anti-Flag (F1804, 1:2000) and anti-GFP (H6908, 1:2000) were purchased from Sigma. Anti-acetylated lysine (clone 4G12, 1:1000) was purchased from Millipore. Anti-NAT10 was a gift from Dr. B. Zhang. For generating anti-Eg5-K771-Ac specific antibody, the peptide "IQQKSK-DIVNKMTFHSQK(Ac) FCADSDG" was synthesized and immunized in New Zealand rabbit by Beijing Jiaxuan zhirui biotechnology.

Co-immunoprecipitation assay

Cell lysates were prepared in Buffer A (25 mM Tris–Cl (pH 7.5), 150 mM KCl, 1 mM DTT, 2 mM EDTA, 0.5 mM PMSF and 0.5% Nonidet P-40) and used directly for immunoprecipitation. Antibodies were coupled with a 50% suspension of protein A-Sepharose beads (GE Healthcare) in IPP500 (500 mM NaCl, 10 mM Tris–Cl (pH 8.0), 0.5% Nonidet P-40), and the coupled beads were incubated with cell lysates for 2 h at 4 °C. After washing, the precipitants were analyzed by Western blot using the indicated antibodies.

RT-qPCR

Total RNA was extracted from cells using TRIzol reagent (Invitrogen) according to the manufacturer's instruction. cDNA was synthesized from 2 μg of total RNA using the Superscript First-Strand Synthesis System (Invitrogen), and qPCR was performed as previously described [30]. The human GAPDH was used as an internal control. All real-time PCR data were analyzed by comparative C_t method and normalized to GAPDH.

In vitro acetylation

Full-length GST-Eg5 or its deletion mutant proteins purified from the *E. Coli.* bacterial cells were used as substrate in the acetylation assay. Flag-NAT10 and Flag-NAT10 G641E were purified from *sf9* cells [30]. Reactions were carried out at 30 °C for 1 h in a reaction containing 50 mM Tris-Cl (pH 7.9), 10% glycerol, 0.1 mM EDTA, 1 mM PMSF, 10 mM sodium butyrate and 10 μM acetyl-CoA at 30 °C for 1 h. Acetylation of target proteins were analyzed by western blot using pan acetyl-lysine specific antibody.

In-cell acetylation assay

Cells were incubated with 1 μm trichostatin A (TSA) and 5 mM nicotinamide (NIA) for 6 h before harvested. Cell extracts were prepared in whole cell lysis buffer (50 mM Tris-HCl (pH 7.8), 137 mM NaCl, 1 mM NaF, 1 mM $NaVO_3$, 1% Triton X-100, 0.2% sarkosyl, 1 mM DTT and 10% glycerol, fresh protease inhibitors, 10 μm TSA and 5 mM NIA) and then incubated with anti-acetyl-lysine antibody-conjugated protein A-Sepharose beads at 4 °C for 2 h. The beads were washed five times with BC100 buffer (50 mM

Tris–HCl (pH 7.8), 100 mM NaCl, 0.2% Triton X-100 and 10% glycerol) as previously described [33]. The immunoprecipitates and total proteins were subjected to Western blot using the indicated antibodies.

Cell cycle analysis

Cell cycle was determined according to the instruction of Cell Cycle Analysis Kit (KeyGen BioTECH, KGA511). Briefly, cells were collected and fixed with 70% ethanol. After washed with PBS for three times, cells were incubated with RNase A and stained with propidium iodide. More than 2×10^4 cells were analyzed using FACSCalibur (Becton Dickinson, Franklin Lakes, NJ, USA) and CellQuest software (Becton Dickinson).

Double thymidine block

Cells were synchronized by double thymidine block as previously described [47]. In brief, cells were plated in 60 mm dishes at 40% confluence at first thymidine block and treated with 5μM thymidine for 19 h. Cells were washed with warm PBS for 2 times and incubated with fresh medium for 9 h. Then, 5μM thymidine was added and incubated for 16 h, cells were released by replacing with fresh medium. Released cells were harvested at 0 h and 8 h and subsequently subjected to cell cycle analysis and immunoblotting.

Immunofluorescence staining

Cells were fixed with 4% paraformaldehyde or cold methanol for 15 mins and permeabilized using 0.2% Triton X-100 for 10 mins at room temperature. After blocking with 10% goat serum, the cells were incubated with the primary antibodies overnight at 4 °C. After washing with PBS, the cells were incubated with FITC-conjugated anti-rabbit antibody or/and TRITC-conjugated anti-mouse antibody for 1 h at room temperature. Finally, the cells were stained with DAPI to visualize the nuclei. Photos were taken under a confocal microscopy (TCS SP8 MP FLIM, Leica, Germany).

Live-cell imaging

Chromosome segregation was assessed in living cells according to previously published methods [48]. The stable cell line HeLa-GFP-H2B-mCherry-tubulin (a gift from D. W. Gerlich, institute of Biochemistry, Swiss Federal Institute of Techonology Zurich, Switzerland) was observed under UltraVIEW VoX (PerkinElmer, USA). The data was recorded every 10 min for 24 h. All live-cell-imaging experiments were performed at least three times as described previously [48].

Centrosome movement and spindle geometry measurements

For measuring centrosome movement in G2 phase and prophase, cells were fixed and stained with pH3S10/γ-tubulin/DAPI. Images were taken under confocal microscopy. The pH3S10 positive cells were defined as mitotic cells [49]. The distance between centrosomes (γ-tubulin signals) was measured using Leica LAS X software (Leica, Germany). Centrosome movement was determined by the ratio of centrosome distance/nuclear diameter, which ≤0.5 were considered as movement delayed [48]. For spindle geometry analysis, maximum intensity optical sections were collected from γ-tubulin/α-tubulin-stained cells using the TCS SP8 MP FLIM confocal microscopy. Leica LAS X software was used to measure the angle between the spindle and the metaphase plate. Cells that had an acute angle between the spindle pole axis and the metaphase plate of less than 85° were considered asymmetrical [48].

RNA interference

For silencing NAT10, siRNA-1 5′-CAGCACCACUGCUGAGAAUAAGA-3′ and siRNA-2 5′-CCGAAUCCGGAUUCUCAUU-3′ were used as described previously [30]. For silencing Eg5, siRNA-1: 5′-CAACAAGGATGAAGTCTAT-3′ and siRNA-2: 5′-CUGAAGACCUGAAGACAAU-3′ were used as described previously [50, 51].

Protein purification

Flag-NAT10-His or its mutants were purified from *sf9* cells as described previously [33]. Briefly, the recombinant baculoviruses were generated with the Bac-to-Bac Baculovirus expression system (Invitrogen). Recombinant proteins were purified from baculovirus-infected *Sf9* cells using Ni-NTA agarose (Qiagen) according to the manufacturer's instructions. Expression of GST fusion proteins or His-Eg5 protein was induced with isopropyl-β-D-thiogalactoside in *E. coli*. strain BL21 (DE3, Tiangen) and the bacteria was lysed by sonication. GST fusion proteins were purified using the Glutathione Sepharose 4B (GE Healthcare) from the bacteria lysates. His-Eg5 was purified by Ni^{2+}-Sepharose affinity (GE Healthcare) and was eluted with 250 mM imidazole in PBS. Purified proteins were resolved by Coomassie Blue staining after separated on SDS-PAGE and were verified by Western blotting probed with corresponding antibodies.

GST pull down assay

GST fusion proteins were prepared following standard protocol [52]. For in vitro binding assay, GST fusion proteins bound to the Glutathione Sepharose 4B (GE Healthcare) were incubated with the Flag-tagged proteins purified from *sf9* cells as described previously [30] or with His-Eg5 protein expressed and purified from *E. coli*. After washing, the GST-fusion protein bound proteins were separated by SDS–PAGE and immunoblotted with anti-Flag antibody.

Protein half-life assay

HeLa cells were transfected with indicated plasmids and treated with cycloheximide (CHX) for 0, 6, 12, 18 and 24 h separately at final concentration of 30 μg/ml. Then the whole cell lysates were prepared and analyzed by Western blotting. Quantification of expression of Eg5 protein under different time points was determined using Image J software and normalized to β-actin.

Cell growth curve

Cell growth was analyzed using MTS reagent (Promega) according to the manufacturer's instruction. Cells were plated on 96 well plates (1000 cells per well) and grown in the media containing 10% serum. MTS was added to the cells, and absorbance at 490 nm was measured at day 0, 1, 2, 3, and 4. Cell growth curve was plotted by absorbance as relative proliferation percentage *v.s.* time points.

Colony formation assay

Cells were seeded into 6 well plates (500 cells per well) and cultured with 10% serum containing media for about 12 days. Cell clones were fixed and stained with crystal violet, and visible colonies were counted.

Identification of acetylation site in Eg5 by LC-MS/MS analysis

In vitro acetylation reaction was resolved on SDS-PAGE. The band of acetylated Eg5 was excised and subjected to in-gel trypsin digestion as previously described [48]. The digested peptides were loaded on a C18-A1 pre-column (100 μm × 2 cm, Thermo Scientific, No. SC100) and subsequently separated on the analytical column (C18-A2, 75 μm × 10 cm, Thermo Scientific, No. SC 200) using an Easy-LC nano-HPLC (Thermo Scientific). For a gradient separation, H2O/FA (99.9:0.1) was used as the mobile phase A, while ACN/FA (99.9:0.1) used was mobile phase B. Mass spectrometric analysis was performed using an LTQ Orbitrap Velos pro (Thermo Scientific, Bremen, Germany). The spray voltage was operated at 2.5 kV with the ion transfer capillary at 250 °C. The MS/MS spectra were obtained in a data-dependent collision induced dissociation (CID) mode, and the full MS was acquired from m/z 350–2000 with resolution 60,000. The top 15 most intense ions were selected for MS/MS. Parameters for acquiring CID were as follows: activation time = 10 ms, normalized energy = 35, Q-activation = 0.25. The dynamic exclusion was set as follows: repeat count 1, duration 30 s, exclusion list size 500 and an exclusion duration 30 s. The analysis of nano-LC-MS/MS was performed by Proteomics Center of Peking University and the mass spectrometry data were processed using the Proteome Discoverer software (Version 1.4).

Nude mice xenograft models

H1299 cells stably transfected with Flag-Eg5, FLag-Eg5-K771R and Flag were established as described previously [20]. These stable cells (5×10^6) were suspended in 200 μL of PBS and injected subcutaneously into the left flank of 4 to 6-week-old male BALB/C nude mice (Beijing Vital River Laboratory Animal Technology Co., Ltd.). After sacrificed at the day 30 post-implantation, tumor size and weight of mice were measured. The tumor volume was calculated using the formula: length × width^2 × 0.5 (mm^3). The group size is the minimum number that is sufficient to establish xenograft mice model. No samples were excluded from the analysis. The experimental intervention and mice were randomized. All animal experiments were approved by the Institutional Animal Care and Use of Peking University Health Science Center.

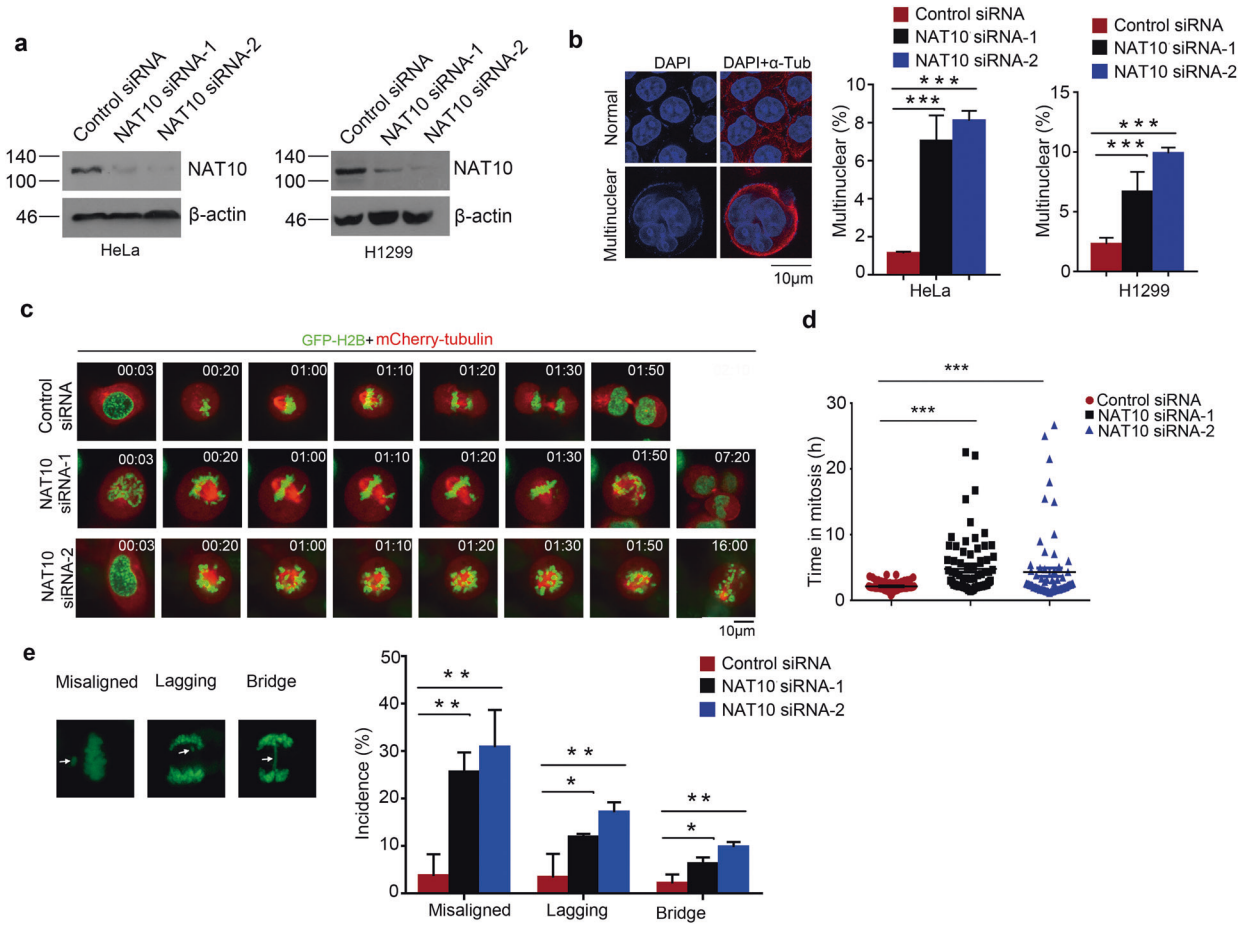

Fig. 1 Knockdown of NAT10 results in chromosome misalignment and defective segregation leading to mitotic catastrophe. a Western blotting was performed on the cell lysates to evaluate NAT10 levels in the siRNA transfected HeLa and H1299 cells. Beta-actin was used as a loading control. **b** HeLa cells and H1299 cells were transfected with NAT10 siRNA or control siRNA. Indirect immunofluorescence staining was performed with anti-tubulin (Red) on the HeLa cells transfected either with NAT10 siRNA or control siRNA. Nucleus was stained with DAPI (left panel). Quantitative comparison of multinuclear cells between control and NAT10 knock down cells is shown ($n = 100$ cells). Data is the average of three independent experiments. Error bars represent standard deviation (SD). *P* value was calculated using one-way ANOVA. ***$P < 0.001$ (right panel). **c** NAT10 siRNA or control siRNA was transfected into the HeLa-H2B-GFP + mCherry-α-tubulin cells. After 48 h, mitosis progression was monitored and recorded under time-lapse fluorescence microscopy. Images were acquired every 10 min. **d** Time duration from nuclear envelope breakdown to anaphase was determined as mitotic time ($n = 50$ cells). Data is the average of three independent experiments as described in (**c**). *P* value was calculated using Kruskal-Wallis test. ***$P < 0.001$. **e** Chromosome misalignment, bridge and lagging in the NAT10-depleted HeLa-H2B-GFP + mCherry-α-tubulin cells (left panel). The frequency of chromosome misalignment, bridge and lagging in NAT10-depleted cells and control cells ($n = 50$). The data is summarized from three independent experiments. Data were analyzed by one-way ANOVA. *$P < 0.05$, **$P < 0.01$ (right panel).

Statistical analysis

Statistical analysis was performed using SPSS software version 25.0 (IBM, Armonk, NY, USA). The post hoc analyses, LSD (Least Significant Difference) test for one-way ANOVA and Tukey's Honest Significant Difference (HSD) test for two-way ANOVA were used to analyze the differences among more than two groups. Kruskal-Wallis test was performed for nonparametric comparison. The group size is the minimum number that is sufficient to define a functional parameter and the variance is similar between the groups. All data met the assumptions of the tests and represented in the figures with the error of the mean (mean ± SD). $p < 0.05$, $p < 0.01$ and $p < 0.001$ were considered statistically significant.

RESULTS

Knockdown of NAT10 results in chromosome misalignment and defective segregation leading to mitotic catastrophe

We observed that depletion of NAT10 in HeLa and H1299 cells leads to increase of giant multiple nuclear cells, which is a hall marker of mitotic catastrophe [3] (Fig. 1a, b; Supplementary Fig. 1). To unravel how NAT10 regulates mitosis, we silenced NAT10 by siRNA in HeLa-GFP-H2B-M-Tub cells which stably express GFP-histone 2B and mCherry-tubulin and monitored the mitotic process using time-lapse image system. Mitosis was completed in 110 mins in the control cells, while knockdown of NAT10 causes defective chromosome segregation which leads to prolonged mitosis till up to 16 h (Fig. 1c, d; Supplemental video). To determine loss of NAT10-caused mitotic disorders, we further examined chromosome segregation in the NAT10-depleted HeLa-GFP-H2B-M-Tub cells. Depletion of NAT10 causes chromosome misalignment, bridge and lagging during mitosis (Fig. 1e). These results demonstrate that loss of NAT10 causes mitotic catastrophe.

NAT10 binds Eg5 and co-localizes with Eg5 at centrosome

To uncover the mechanism by which NAT10 regulates mitosis, we analyzed NAT10-interacting proteins identified by mass spectrometry of Flag-NAT10-specific complex from HCT116 and HeLa cells [30] (Fig. 2a). Among the NAT10 binding proteins in both HCT116 and HeLa cells (Supplementary Fig. 2a), Eg5 is of our special interest as it plays a critical role in the dynamic assembly and

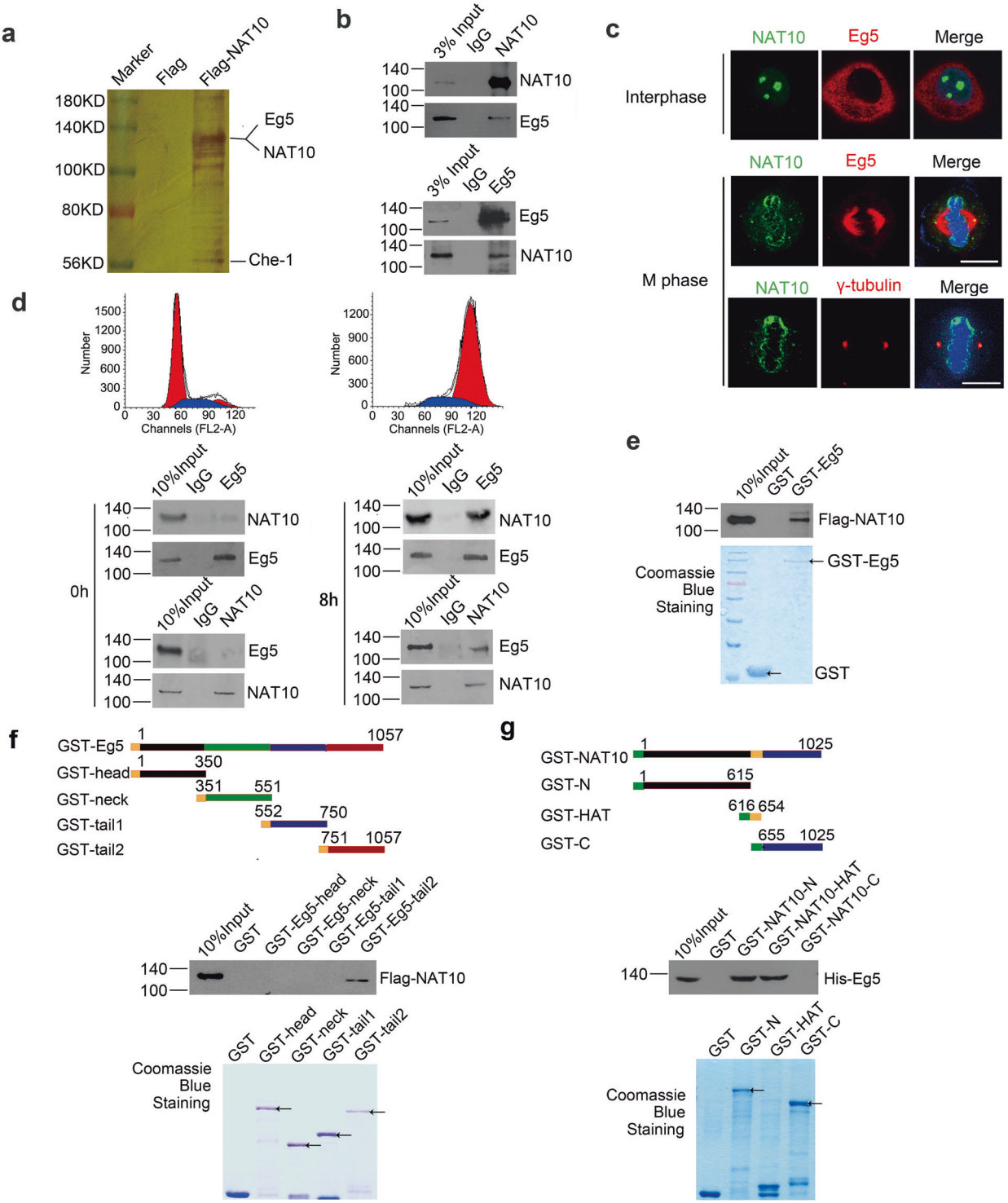

function of the mitotic spindle [53]. The endogenous NAT10-Eg5 interaction was confirmed by immunoprecipitation experiments performed with either anti-NAT10 or anti-Eg5 antibody on the cellular extracts from HeLa, H1299 and HCT116 cells (Fig. 2b; Supplementary Fig. 2b). To obtain the functional insight into the association between NAT10 and Eg5, we examined the cellular localization of NAT10 and Eg5. Immunofluorescence staining shows that in the interphase, NAT10 predominantly localizes in the nucleolus, while Eg5 mainly localizes in the cytoplasm. However, in mitotic cells, when the chromatin is condensed, NAT10 is co-localized with Eg5 at spindle poles (Fig. 2c; Supplementary Fig. 2c). In addition, Eg5 stretched from the centrosome to the spindle filaments as described previously [54], while NAT10 wraps the chromosomes in the metaphase (Fig. 2c, Supplementary Fig. 2d). These results confirmed that NAT10 interacts with Eg5 in the centrosomes during mitosis. To verify the physical interaction and co-localization between NAT10 and Eg5 during mitosis, co-immunoprecipitation was performed in interphase cells and mitotic cells. HeLa cells were synchronized using double thymidine blocking and cells in G1/S and G2/M phase

Fig. 2 NAT10 binds Eg5 and colocalizes with Eg5 at centrosome. a HeLa cells were transfected with Flag-NAT10 or Flag control vector. Whole-cell extracts were immunoprecipitated with anti-Flag antibody affinity resin. The NAT10-binding proteins were resolved by SDS–PAGE and silver staining. **b** Immunoprecipitation was performed on the HeLa cell lysates using indicated antibodies. The immunoprecipitates were subsequently immunoblotted with the indicated antibodies. **c** Immunofluorescence staining was done with indicated antibodies to show the localization of endogenous NAT10, Eg5 and γ-tubulin. Chromosomes were stained with DAPI. Bar represents 10 μm. **d** HeLa cells were synchronized using double thymidine blocking and cells were collected at G1/S phase and M phase. Cell cycle was determined by flow cytometry (upper). Immunoprecipitation was performed on the HeLa cell lysates using indicated antibodies. The immunoprecipitates were immunoblotted with the indicated antibodies (lower). **e** GST pull-down experiment was performed with purified GST-Eg5 and Flag-NAT10. The binding of Flag-NAT10 to GST-Eg5 was detected by immunoblotting with anti-Flag antibody (upper). The purified GST or GST-Eg5 proteins were resolved by SDS–PAGE and stained by Coomassie Blue (lower). **f** The schematic diagram represents the GST-Eg5 deletion mutant constructs (upper). GST pull-down experiment was performed using purified GST or GST-Eg5 deletion mutants with purified Flag-NAT10 (lower panel). The purified GST or GST-Eg5 proteins were resolved by SDS–PAGE and stained by Coomassie Blue (lowest panel). **g** The schematic diagram represents the GST-NAT10 deletion mutant constructs (upper). GST pull-down experiment was performed using purified GST or GST-NAT10 deletion mutants with purified His-Eg5 (lower panel). The purified GST or GST-NAT10 proteins were resolved by SDS–PAGE and stained by Coomassie Blue (lowest panel).

were collected at 0 h and 8 h after release, respectively (Fig. 2d). Immunoprecipitation results indicated that NAT10 interacts with Eg5 in mitotic cells, but not in interphase cells (Fig. 2d).

To determine if NAT10 directly interacts with Eg5, GST pulldown experiments were performed with Flag-NAT10 purified from *sf9* insect cells and GST-Eg5 proteins purified from *E. Coli*. Purified Flag-NAT10 interacts with GST-Eg5 in vitro (Fig. 2e). Moreover, the NAT10-binding region of Eg5 was narrowed down to the tail2-terminal domain (Fig. 2f). To map the Eg5-binding domain in NAT10, GST pull down experiments were performed with purified His-Eg5 (Supplementary 2e) and GST-NAT10 deletion mutants (Fig. 2g). NAT10 binds Eg5 with the N domain and HAT domain which contains the acetyltransferase activity, suggesting that NAT10 might regulate Eg5 through its acetyltransferase function.

NAT10 regulates the poleward movement of centrosome probably through controlling centrosome loading of Eg5

Since Eg5 plays essential roles in the bipolar spindle formation by controlling centrosome movement and spindle geometry [55], we wanted to know if NAT10 affects bipolar spindle formation. We found that NAT10 depletion by siRNAs in HeLa cells increased monopolar spindles by 3.2 and 3.4 folds (38.5% v.s. 12% and 41% v.s. 12%), while Eg5 depletion increased monopolar spindles by 4.0 and 4.4 folds (68% v.s. 17% and 75% v.s. 17%). Similarly, NAT10 depletion by siRNAs in H1299 cells increased monopolar spindles by 3.8 and 4.3-folds (38% v.s. 10% and 43% v.s. 10%), while Eg5 depletion increased monopolar spindles by 7.0 and 8.2-folds (70% v.s. 10% and 82% v.s. 10%). (Fig. 3a–c). In addition, knockdown of NAT10 in HeLa cells resulted in a significant increase of cells with asymmetric spindle by 2.0 and 2.4 folds (16% v.s. 8% and 19% v.s. 8%), while Eg5 depletion increased asymmetric spindle by 4.1 and 3.4 folds (32.5% v.s. 8.0% and 27.0% v.s. 8.0%). Knockdown of NAT10 in H1299 cells resulted in a significant increase of cells with asymmetric spindle by 2.5 and 2.0 folds (25% v.s. 10% and 20% v.s. 10%), while Eg5 depletion increased asymmetric spindle by 3.5 and 4 folds (35% v.s. 10% and 40% v.s. 10%) (Fig. 3d, e). These data indicate that NAT10 plays similar roles as Eg5 does in mitosis. Since Eg5 governs the centrosome movement during mitosis, we silenced NAT10 and measured the poleward movement by the ratio of centrosome distance/nuclear diameter in the G2 phase as described previously [48]. Depletion of NAT10 in HeLa cells increased the retarded centrosome movement by 2.8 and 2.9 folds (28% v.s. 10% and 29% v.s. 10%), while knockdown of Eg5 increased the retarded centrosome movement by 4.5 and 5.4 folds (45% v.s. 10% and 54% v.s. 10%). Depletion of NAT10 in H1299 cells increased the retarded centrosome movement by 4.4 and 3.1 folds (35% v.s. 8% and 25% v.s. 8%), while knockdown of Eg5 increased the retarded centrosome movement by 7.0 and 7.3-folds (56% v.s. 8% and 59% v.s. 8%) (Fig. 3f, g). These results suggest that NAT10 controls the poleward movement of centrosomes probably through regulating Eg5. Given that Eg5 functions in the bipolar formation by loading to the centrosomes during mitosis [15], we next determined if NAT10 regulates the centrosome loading of Eg5. Depletion of NAT10 strikingly reduced centrosome loading of Eg5 (Fig. 3h, i). These results indicate that NAT10 might regulate the poleward movement of centrosomes through controlling centrosome loading of Eg5.

NAT10 stabilizes Eg5 dependent on its acetyltransferase activity

To unravel how NAT10 regulates the function of Eg5, we evaluated Eg5 levels when NAT10 was depleted. We show that knockdown of NAT10 by siRNAs decreased Eg5 protein levels in HeLa and H1299 cells without changing the Eg5 mRNA level (Fig. 4a; Supplementary Fig. 3a, b), suggesting that NAT10 regulates Eg5 level through protein-protein interaction rather than transcriptional regulation. To rule out the off-target effect of NAT10 siRNAs, the protein levels of Eg5 were evaluated in *NAT10* KO cells (C4 & C19) generated by genome editing (Supplementary Fig. 3c, d). Knockout of *NAT10* in C4 and C19 cells also decreased protein levels of Eg5 (Fig. 4b). Accordingly, ectopic expression of Flag-NAT10 results in a dose-dependent increase of Eg5 protein levels in HeLa and H1299 cells (Fig. 4c left; Supplementary Fig. 3e) without changing Eg5 mRNA levels (Fig. 4c right; Supplementary Fig. 3f), confirming NAT10 regulates Eg5 levels through protein-protein interaction. Importantly, the enzyme-dead mutant Flag-NAT10 G641E fails to elevate Eg5 protein levels (Fig. 4d), indicating that the acetyltransferase activity of NAT10 is required for regulating Eg5. In addition, the NAT10-specific inhibitor Remodelin caused a dose-dependent decrease of Eg5 protein levels (Fig. 4e; Supplementary Fig. 3g), further confirming that NAT10 regulates Eg5 protein level depending on its acetyltransferase activity. Inhibition of proteasome by MG132 blocked the Eg5 decrease caused by depletion of NAT10, indicating that NAT10 may protect Eg5 from the proteasomal degradation (Fig. 4f). Next, we show that depletion of NAT10 by siRNA dramatically shortened the half-life of Eg5 (Fig. 4g). In accordance, Flag-NAT10 prolonged half-life of Eg5 (Fig. 4h). However, Flag-NAT10 G641E mutant fails to regulate Eg5 protein stability (Fig. 4h). Taken together, our data indicate that NAT10 regulates Eg5 protein stability dependent on its acetyltransferase activity.

Eg5 is acetylated by NAT10 at lysine 771

To determine if NAT10 acetylates Eg5, in vitro acetylation experiment was performed with purified Flag-NAT10 and GST-Eg5. Flag-NAT10 acetylates GST-Eg5 in the presence of acetyl-CoA in vitro (Fig. 5a). In addition, the acetylation level of Eg5 decreased in the HeLa-NAT10-KO cells (Fig. 5b). Furthermore, Flag-NAT10 acetylates GFP-Eg5 in cells, while Flag-NAT10-G641E fails to do so (Fig. 5c), confirming that Eg5 is acetylated by NAT10. These data demonstrate that NAT10 is a bona fide acetyltransferase for Eg5.

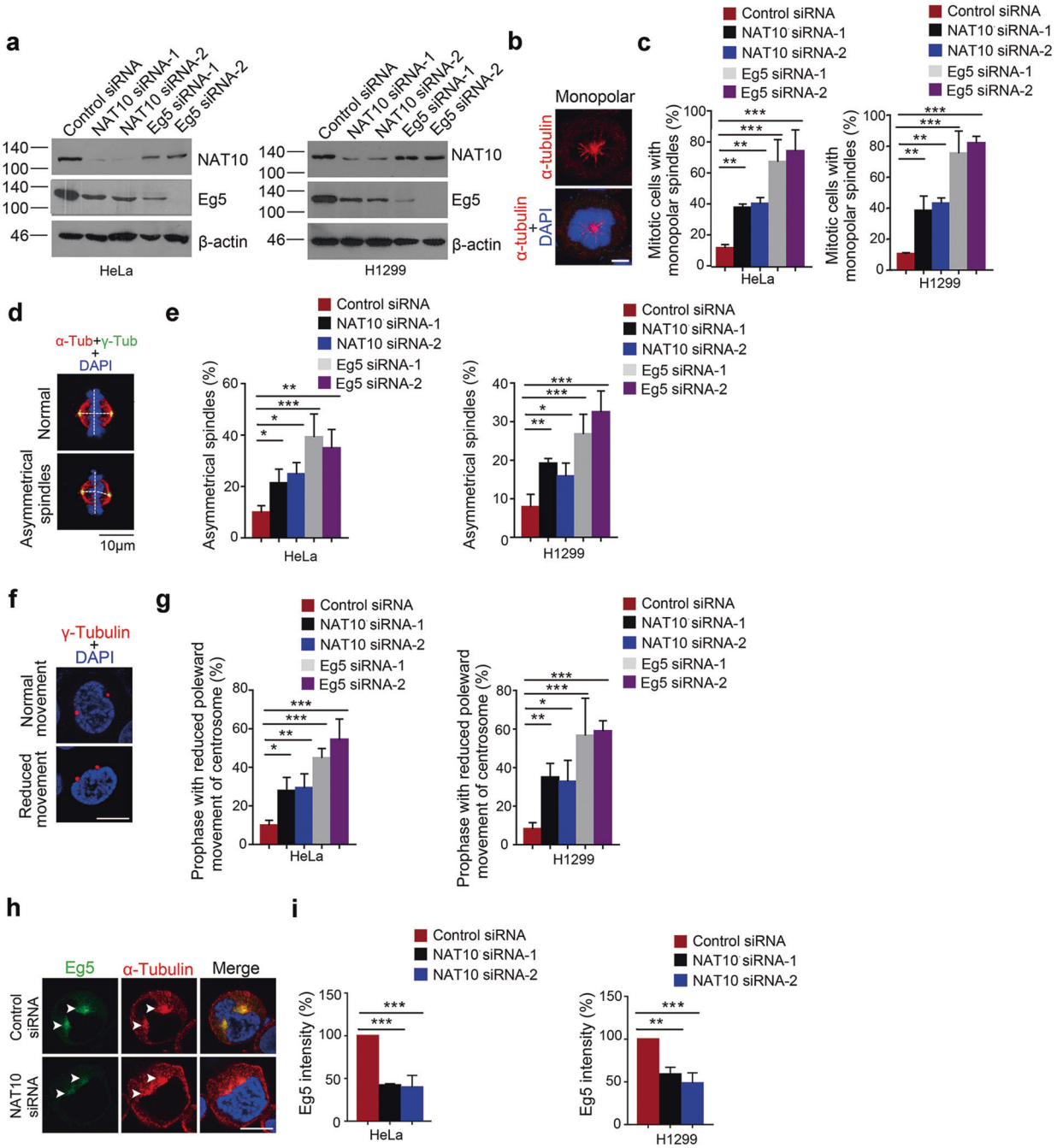

Fig. 3 NAT10 regulates poleward movement through controlling centrosome loading of Eg5. a HeLa cells were transfected with indicated siRNAs. Western blotting was performed on the cell lysates to evaluate NAT10 and Eg5 levels. Beta-actin was used as a loading control. **b** Mitotic spindles are visualized by immunofluorescence staining using α-tubulin antibody (red) in the cells as described in a. Chromosomes are stained with DAPI (blue). Shown is a representative image of monopolar spindle. Bar = 10 μm. **c** The percentages of mitotic HeLa cells (left panel) and H1299 cells (right panel) with a monopolar spindle were determined ($n = 50$ cells). Data are averages of three independent experiments. Error bars represent standard deviation (SD). *P* values were calculated using one-way ANOVA. $^{**}P < 0.01$, $^{***}P < 0.001$. **d** Immunofluorescence staining was performed to visualize mitotic spindle (α-tubulin, red) and spindle poles (γ-tubulin, green). Chromosomes were stained with DAPI (blue). Shown is a representative image of asymmetric spindle. Scale bar represents 10 μm. **e** The percentage of asymmetrical spindles in NAT10-depleted cells and control cells ($n = 25$ cells). Data is the average of three independent experiments. *P* values were calculated using one-way ANOVA. $^{*}P < 0.05$, $^{**}P < 0.01$, $^{***}P < 0.001$. **f** Centrosomes were stained with anti-γ-tubulin (red) and DNA was stained with DAPI (blue). Centrosome movement in prophase cells were determined by dividing the distance between centrosomes by the diameter of the nucleus. Shown is a representative image of reduced centrosome movement. **g** The percentages of reduced centrosome movement (the ratio < 0.5) in prophase cells of HeLa (left panel) and H1299 (right panel) were calculated ($n = 25$ cells). Data are averages of three independent experiments. *P*-values were calculated using one-way ANOVA. $^{*}P < 0.05$, $^{**}P < 0.01$, $^{***}P < 0.001$. **h** Immunofluorescence staining was performed to visualize Eg5 (green) and α-tubulin (red) in the HeLa and H1299 cells described in (**a**). DNA was stained with DAPI (blue). **i** The intensity of Eg5 signal at centrosomes was determined by scanning with Leica LAS X confocal software ($n = 25$). The relative Eg5 intensity standardized by α-tubulin in the control cells was assigned as 100%. Data are averages of three independent experiments. *P* values were calculated using one-way ANOVA. $^{**}P < 0.01$, $^{***}P < 0.001$.

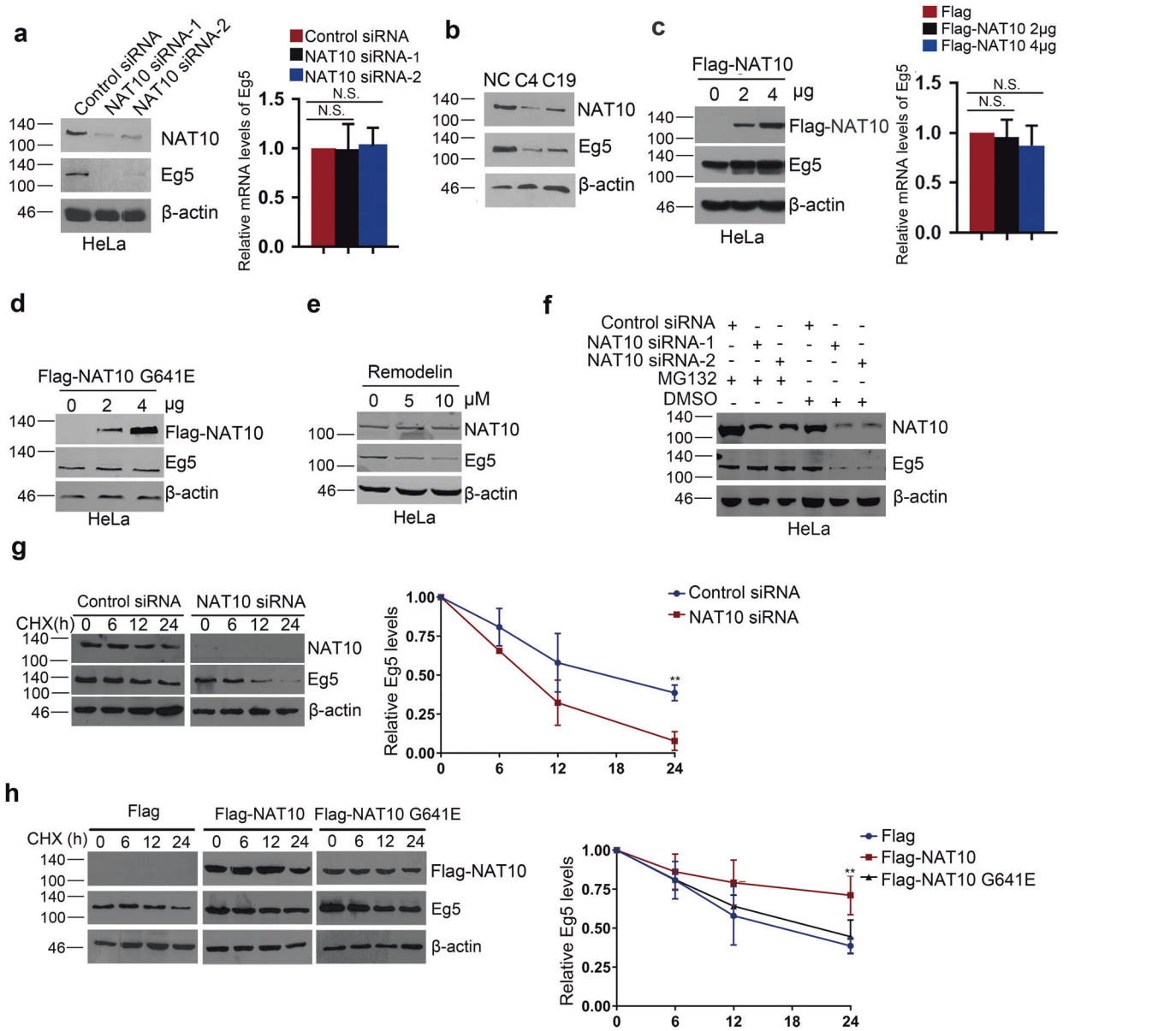

Fig. 4 NAT10 stabilizes Eg5 dependent on its acetyltransferase activity. a HeLa cells were transfected with the indicated siRNAs. NAT10 and Eg5 levels were evaluated by Western blot (left panel). Beta-actin was used as a loading control. Eg5 mRNA level was evaluated by RT-qPCR (right panel). *P* values were calculated using one-way ANOVA. N.S. denotes no significance. **b** CRISPR-Cas9 system-mediated gene editing was applied to knockdown *NAT10* in HeLa cells as described in "Materials and Methods". Cell lysates were prepared from the *NAT10*-depleted cells (C4 and C19) and control cells (NC). Western blot was performed on the cell lysates for the evaluation of the indicated proteins. **c** HeLa cells were transfected with increasing amounts of NAT10 plasmid. Immunoblot was performed on the cell lysates using the indicated antibodies (left panel). Eg5 mRNA level was evaluated by RT-qPCR (right panel). *P* values were calculated using one-way ANOVA. N.S. denotes no significance**. d** HeLa cells were transfected with increasing amounts of NAT10G641E plasmid. Immunoblot was performed on the cell lysates using the indicated antibodies. **e** HeLa cells were treated with different concentration of Remodelin (0, 5, 10 μM). After 48 h, proteins from cell lysates were subjected to immunoblot analysis using the indicated antibodies. **f** HeLa cells were transfected with the indicated siRNAs and treated with DMSO or MG132 10 μM for 6 h before harvest, proteins from cell lysates were subjected to immunoblot analysis using the indicated antibodies. **g** HeLa cells were transfected with NAT10 siRNA or control siRNA. Forty-eight hours later, cells were treated with cycloheximide (CHX) and harvested at the indicated time points. Proteins from cell lysates were subjected to immunoblot for the evaluation of NAT10 and Eg5 (left panel). Relative Eg5 protein levels standardized by beta-actin at different time points are plotted (right panel). Shown are the averages of three independent experiments in triplicates. Error bars represent the SEM. Data were analyzed by 2-way ANOVA. $^{**}P < 0.01$. **h** HeLa cells were transfected with Flag, Flag-NAT10 or Flag-NAT10 G641E and harvested at indicated time points after treatment with CHX. Proteins from cell lysates were immunoblotted with the antibodies as indicated (left panel). Relative Eg5 protein levels standardized by beta-actin at different time points are shown in the right. Shown are the averages of three independent experiments in triplicates. Error bars represent the SEM. Data were analyzed by 2-way ANOVA. $^{**}P < 0.01$.

We further determined the acetylation sites of Eg5 catalyzed by NAT10. The acetylation sites of Eg5 was determined by mass spectrometric analysis after in vitro acetylation experiment was performed using purified GST-Eg5 and Flag-NAT10. Eg5 is acetylated by NAT10 at lysine 771 which is conserved in higher species (Fig. 5d; Supplementary Fig. 4a), suggesting that K771 might be required for Eg5 function. The site-directed Eg5 mutant GST-Eg5-K771R was constructed and purified from *E. Coli*. In vitro acetylation experiment

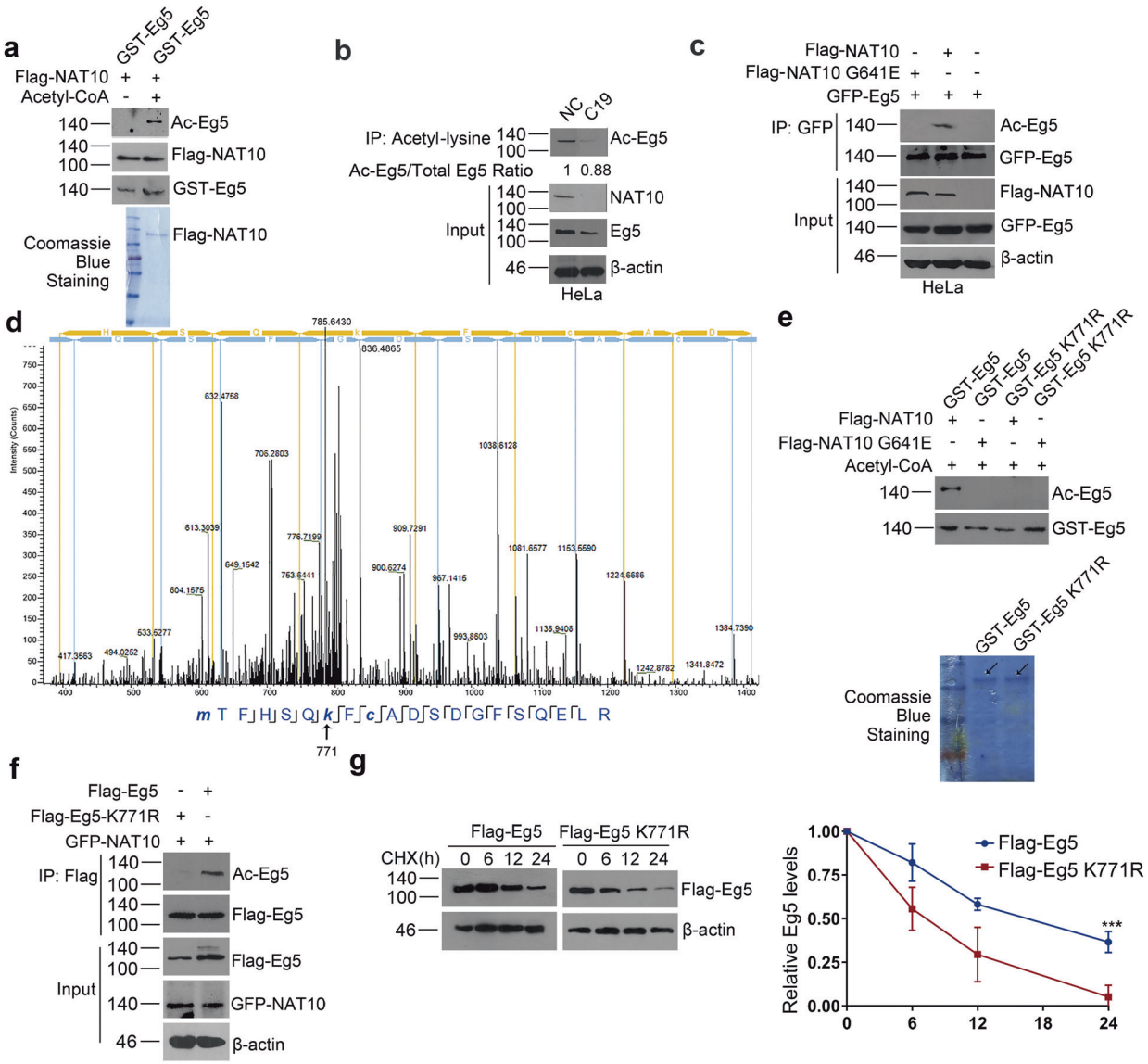

Fig. 5 Eg5 is acetylated by NAT10 at lysine 771. a In vitro acetylation was performed with recombinant GST-Eg5 and purified Flag-NAT10 with or without acetyl-CoA as described in "Materials and Methods". The reaction products were resolved by SDS-PAGE and immunoblotted using anti-acetyl-lysine, anti-Flag or anti-GST antibodies. **b** The *NAT10*-KO HeLa cell (C19) and control cells (NC) were harvested. Cell lysates were prepared and subjected to immunoprecipitation using anti-acetyl-lysine antibody. The acetylation levels of Eg5 were evaluated by Western blot using anti-Eg5 antibody. **c** HeLa cells were transfected with the indicated plasmids. Total proteins were immunoprecipitated with anti-GFP antibody and the acetylation of Eg5 was evaluated by anti-acetyl-lysine antibody (upper). Expression of GFP-Eg5 and Flag-NAT10 were analyzed by Western blot using the indicated antibodies (lower). **d** In vitro acetylation assay was performed as described in (**a**). The reaction products were resolved by SDS-PAGE. The band of acetylated Eg5 was cut, fully trypsinized and analyzed by LC-MS/MS using mass spectrometer (Thermo). Mass spectrometry data were processed using the Proteome Discoverer software (Version 1.4). **e** In vitro acetylation was performed with purified GST-Eg5 or GST Eg5-K771R fusion proteins and purified Flag-NAT10 or Flag-NAT10 GE proteins as described in "Materials and Methods". GST-Eg5 proteins were pulled down with Glutathione sepharose 4B from the reaction mixtures and subjected to Western blot using anti-acetyl-lysine antibody. **f** HeLa cells were transfected with the indicated vectors. Total proteins from cell lysates were immunoprecipitated with anti-Flag antibody and acetylation of Eg5 was evaluated by anti-acetyl-lysine antibody. **g** HeLa cells were transfected with the indicated constructs. Cells were harvested after CHX treatment for the indicated times and cell lysates were prepared. Flag-Eg5 protein levels were evaluated by Western blot. Relative Flag-Eg5 protein levels standardized by β-actin at different time points are shown in the right. Data were analyzed by 2-way ANOVA. ***$P < 0.001$.

shows that GST-Eg5 is acetylated by Flag-NAT10 but not by Flag-NAT10 G641E, while GST-Eg5-K771R is not acetylated by Flag-NAT10 (Fig. 5e; Supplementary Fig. 4b). In addition, in cell acetylation experiments shows that Flag-Eg5 but not Flag-Eg5-K771R is acetylated by GFP-NAT10 (Fig. 5f), demonstrating NAT10 acetylates Eg5 at K771. Furthermore, the protein stability of Flag-Eg5-K771R is dramatically reduced compared to Flag-Eg5 (Fig. 5g). In accordance, the poly-ubiquitination of Flag-Eg5-K771R is significantly increased compared to Flag-Eg5 (Supplementary Fig. 5a), indicating that NAT10 stabilizes Eg5 through acetylation at K771. Additionally, inhibition of NAT10 function by Remodelin enhances poly-ubiquitination of Flag-Eg5 but not Flag-Eg5-K771R (Supplementary Fig. 5b). Collectively, we demonstrate that NAT10 stabilizes Eg5 through acetylating Eg5 at K771.

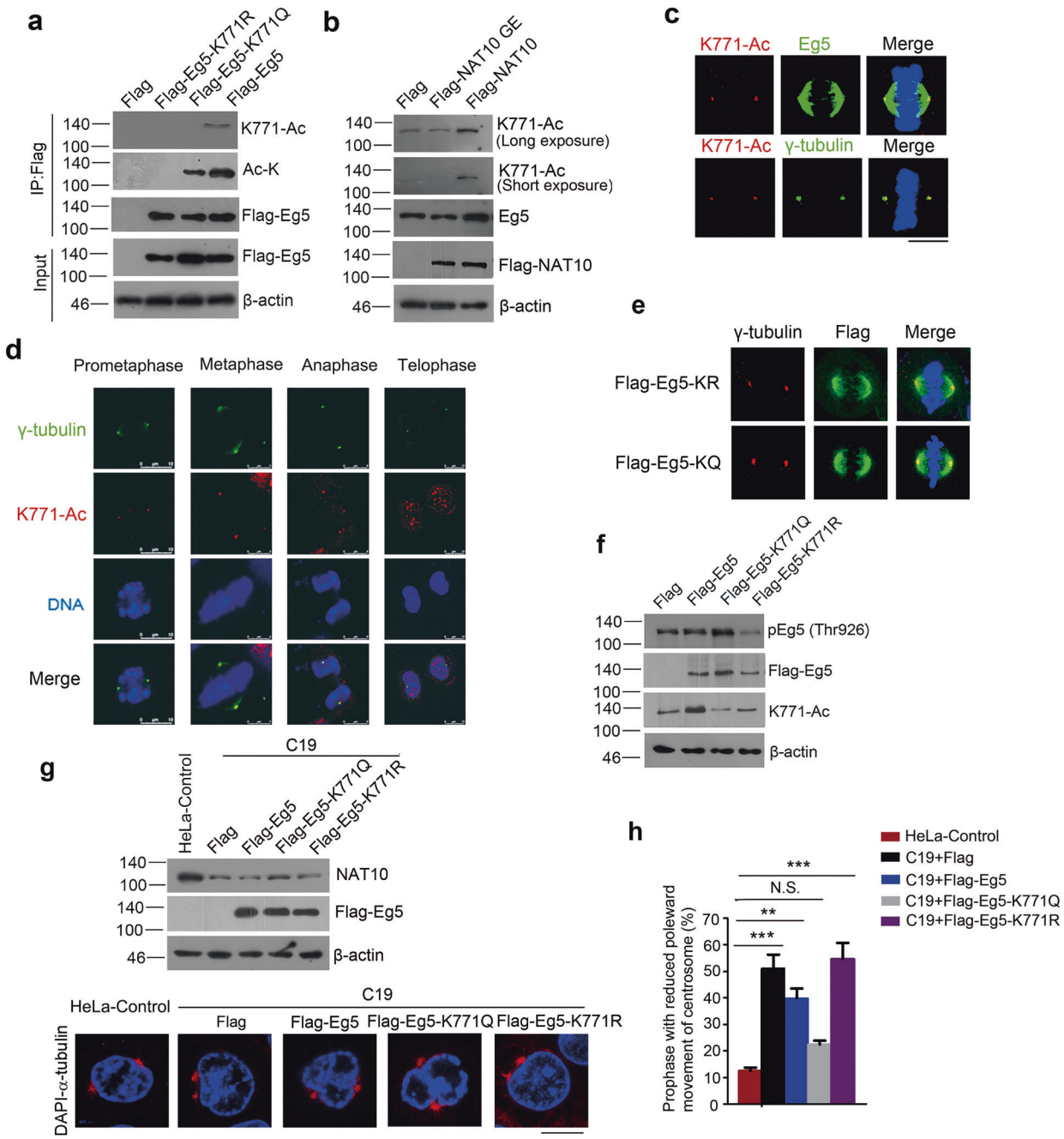

Fig. 6 Eg5 K771-Ac is required for the poleward movement. a HeLa cells were transfected with the indicated vectors. Total proteins from cell lysates were immunoprecipitated with anti-Flag antibody and acetylation of Eg5 was evaluated by Eg5 K771-Ac antibody or anti-acetyl-lysine antibody (Ac-K). **b** HeLa cells were transfected with the indicated vectors. Western blot was performed with indicated antibodies on the cell lysates. Beta-actin was evaluated as a loading control. **c** Immunofluorescence staining was performed with anti-Eg5 K771-Ac antibody (red) and anti-Eg5 (green) or anti-γ-tubulin antibody (green). The nucleus was stained with DAPI (blue). Scale bar represents 10 μm. **d** Immunofluorescence staining was performed with anti-Eg5 K771-Ac antibody (red) and anti-γ-tubulin antibody (green). The nucleus was stained with DAPI (blue). **e** HeLa cells were transfected with Flag-Eg5 K771R or Flag-Eg5 K771Q. Immunofluorescence staining was performed with anti-γ-tubulin antibody (red) and anti-Flag antibody (green) on the transfected cells. The nucleus was stained with DAPI (blue). Scale bar represents 10 μm. **f** Cell lysates were prepared from the HeLa cells stably expressing Flag, Flag-Eg5, Flag-Eg5 K771Q or Flag-Eg5 K771R. Western blot was performed on the cell lysates with indicated antibodies. **g** Different plasmids was ectopically expressed in HeLa-C19 cells. Western blot was performed on the cell lysates to evaluate the expression levels of indicated proteins (upper). Immunofluorescence staining was performed with anti-α-tubulin (red) to indicate centrosomes and nucleus was stained with DAPI (blue) (lower). Centrosome movement in prophase cells were determined by dividing the distance between centrosomes by the diameter of the nucleus. Shown are representative images. **h** The percentages of reduced centrosome movement (the ratio < 0.5) in prophase cells were calculated ($n = 25$ cells). Data are averages of centrosome movement summarized from three independent experiments. *P* values were calculated using one-way ANOVA. $^{**}P < 0.01$, $^{***}P < 0.001$, N.S. denotes no significance.

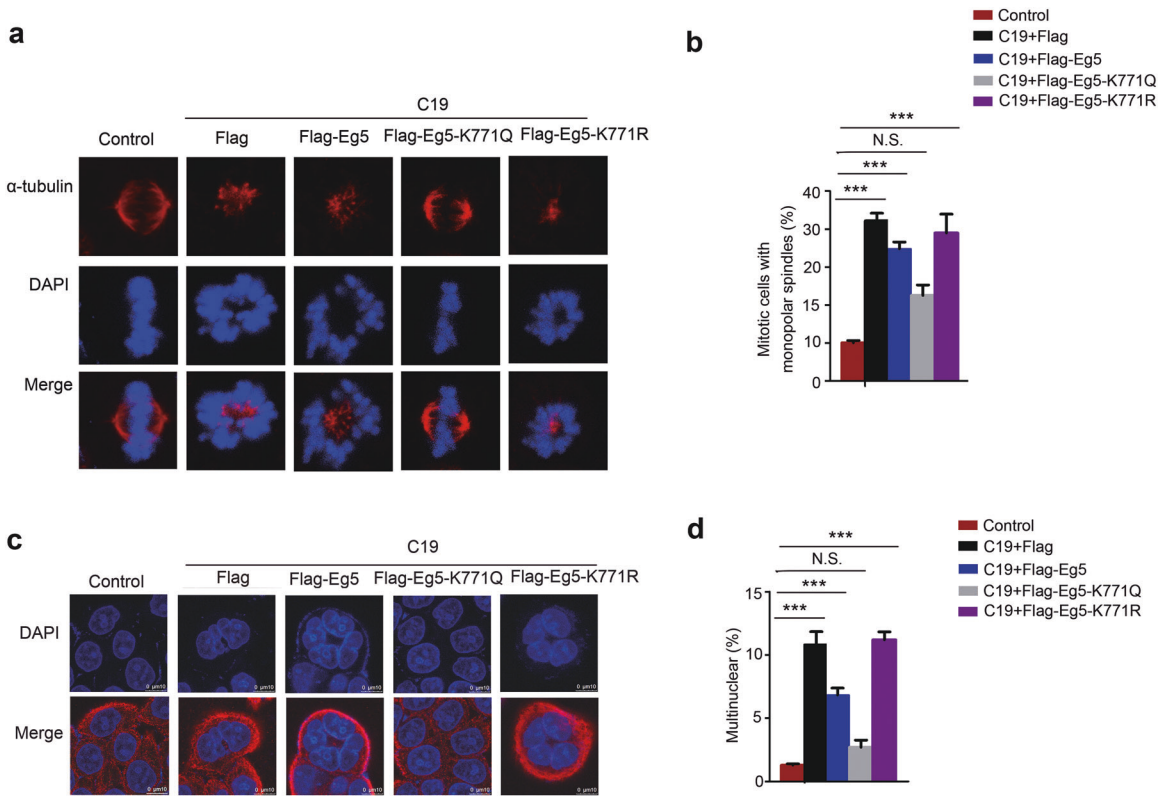

Fig. 7 NAT10 deficiency-caused defective spindle formation and mitotic catastrophe are rescued by Flag-Eg5 K771Q. a HeLa-C19 cells were transfected with Flag, Flag-Eg5, Flag-Eg5 K771Q or Flag-Eg5 K771R. Alpha-tubulin (Red) was visualized by indirect immunofluorescence. Nucleus was stained with DAPI. Scale bar represents 10 μm. **b** The percentage of cells with monopolar spindle were shown ($n = 25$ cells). Data are the averages of three independent experiments in triplicates. Error bars represent the SEM. *P* values were calculated using one-way ANOVA. ***$P < 0.001$. N.S. denotes no significance. **c** Indirect immunofluorescence staining was performed with anti-α-tubulin (Red) on the HeLa-C19 cells transfected with indicated plasmids. Nucleus was stained with DAPI. Scale bar represents 10 μm. **d** The percentages of cells with multinuclear cells were determined ($n = 100$ cells). Data are averages of three independent experiments in triplicates. Error bars represent the SEM. *P* values were calculated using one-way ANOVA. ***$P < 0.001$. N.S. denotes no significance.

Eg5-K771-Ac is required for the poleward movement of centrosome

To further evaluate the role of K771 acetylation on Eg5 function, we generated K771-acetylation specific antibody (designated as "K771-Ac") to recognize the K771 acetylation. The specificity of K771-Ac antibody was verified by Dot blotting (Supplementary Fig. 6). The K771-Ac antibody detects acetylated Eg5 band in the immunoprecipitated Flag-Eg5 but not in the immunoprecipitaed Flag-Eg5 K771R or K771Q (lysine to glutamine mutant for protein hyperacetylation mimic) (Fig. 6a), indicating that K771-Ac specifically recognizes K771-acetylated Eg5. Furthermore, Flag-NAT10 enhances the acetylation of endogenous Eg5 at K771 in cells while Flag-NAT10 G641E fails to do so (Fig. 6b). Taken together, these data demonstrate that NAT10 acetylates endogenous Eg5 at K771 in cells. Importantly, immunofluorescence staining performed with K771-Ac antibody showed that Eg5 K771-Ac specifically locates at the centrosomes during mitosis (Fig. 6c), demonstrating that K771 acetylation predominantly functions in the centrosomes during mitosis. This is further confirmed by the immunofluorescence staining which shows that Eg5 K771-Ac co-localizes with γ-tubulin in the centrosomes from pro-metaphase to telophase (Fig. 6d).

Since the phosphorylation of Eg5 at Thr926 (pEg5-Thr926) controls the poleward movement of Eg5, we determined if Eg5 K771-Ac affects pEg5-Thr926 level. We show that the pEg5-Thr926 level dramatically decreased in the cells expressing Flag-K771R, and increased in the cells expressing Flag-K771Q (Fig. 6f) though both Flag-Eg5 K771R and Flag-Eg5-K771Q localize at the spindle poles during mitosis (Fig. 6e), indicating that K771-Ac is required for the phosphorylation of Eg5-Thr926 and might control the poleward movement. Indeed, in HeLa-C19 cells, the NAT10-KO-retarded poleward movement was rescued by Flag-Eg5-K771Q, but not by either Flag-Eg5 or Flag-Eg5 K771R (Fig. 6g, h), demonstrating that Eg5-K771-Ac is required for the poleward movement of centrosome.

The NAT10 depletion-caused defective spindle formation and mitotic catastrophe were rescued by the hyper-acetylation mimic Flag-Eg5K771Q but not Flag-Eg5

To determine the functional effect of Eg5 K771-Ac in the spindle formation, we ectopically expressed Flag, Flag-Eg5, Flag-Eg5 K771R and Flag-Eg5-K771Q in HeLa-C19 cells, respectively. We found that only Flag-Eg5 K771Q rescues the NAT10-KO induced mono-polar spindle formation (Fig. 7a, b). Consequently, Flag-Eg5 K771Q rescues mitotic catastrophe in HeLa-C19 cells (Fig. 7c, d), while either Flag-Eg5 or Flag-Eg5 K771R fails to do so. These findings demonstrate that NAT10 maintains proper mitosis through acetylating Eg5 K771.

Block of NAT10 or Eg5 function inhibits cell proliferation

To determine if loss of either NAT10 function or Eg5 function affects cell proliferation, MTT and colony formation were performed after cells were treated with Remodelin or S-trityl-l-cysteine (STLC). STLC is an Eg5 inhibitor and suppresses activity of Eg5 ATPase. Either Remodelin or STLC inhibits cell proliferation in HeLa and H1299 cells (Fig. 8a, b, Supplementary Fig. 8a, b). To determine if acetylation of Eg5 K771 is required for cell

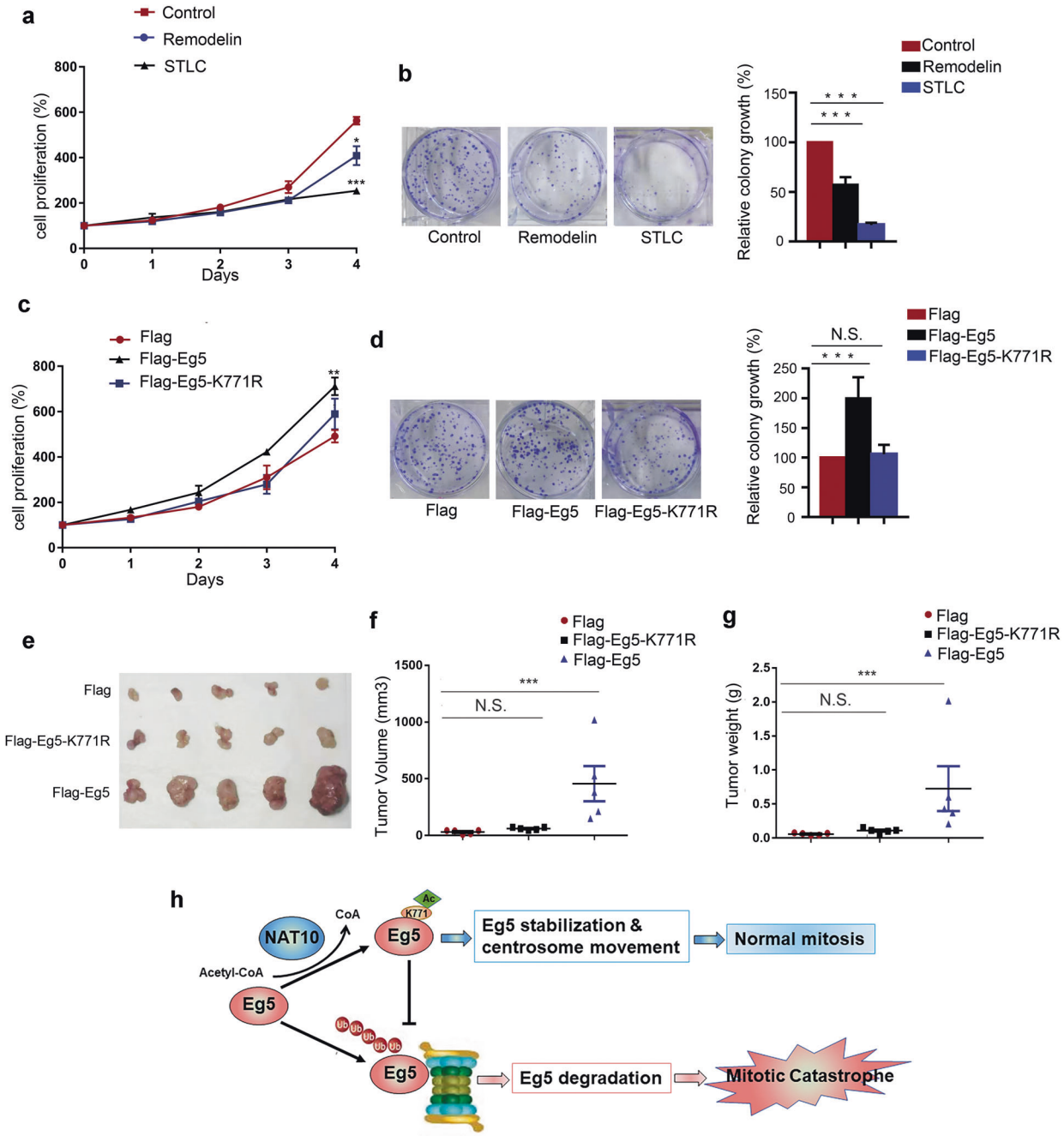

Fig. 8 Repression of NAT10 or Eg5 function inhibits cell proliferation. a HeLa cell lines were treated with DMSO, Remodelin (2.5 mM) or STLC (5 mM). Cell growth curves were plotted by MTT assay. Data were analyzed by 2-way ANOVA. $^{*}P < 0.05$, $^{***}P < 0.001$. **b** Colony formation assay was performed with HeLa cells treated with DMSO, Remodelin or STLC as described in (**a**) (left). Formed colonies were calculated from three independent experiments in triplicates. *P* values were calculated using one-way ANOVA. Error bars represent the SEM (right). $^{***}P < 0.001$. **c** HeLa cells were stably transfected with Flag, Flag-Eg5, or Flag-Eg5-K771R. Cell growth curves were plotted by MTT assay. Data were analyzed by 2-way ANOVA. $^{**}P < 0.01$. **d** Colony formation assay was performed with HeLa cells stably transfected with Flag-Eg5 or Flag-Eg5-K771R (left). Formed colonies were calculated from three independent experiments in triplicates (right). Error bars represent the SEM (one-way ANOVA). $^{***}P < 0.001$. N.S. denotes no significance. **e** H1299 cells stably transfected with Flag-Eg5 or Flag-Eg5-K771R cells were subcutaneously implanted into nude mice. Tumors were dissected at the end of the experiment. **f** The weights of the tumor xenografts are shown, respectively. Error bars indicate the SEM ($n = 6$). Data were analyzed by Kruskall-Wallis test, $^{***}P < 0.001$, N.S. denotes no significance. **g** The sizes of the tumor xenografts are shown. Error bars indicate the SEM ($n = 6$). Data were analyzed by Kruskall-Wallis test, $^{***}P < 0.001$, N.S. denotes no significance. **h** A working model explaining the mechanism by which loss of NAT10 leads to mitotic catastrophe.

proliferation, Flag-Eg5 or Flag-Eg5 K771R was ectopically expressed in HeLa and H1299 cells. Flag-Eg5-K771R fails to promote cell proliferation as Flag-Eg5 does (Fig. 8c, d, Supplementary Fig. 8c, d), manifesting that acetylation at K771 is required for the function of Eg5 in cell proliferation. To further confirm the function of Eg5-K771R in vivo, we subcutaneously implanted H1299 cells stably expressing Flag, Flag-Eg5 or Flag-Eg5-K771R into nude mice. Flag-Eg5 promotes tumor growth in xenograft mice model, while Flag-Eg5-K771R loses this function (Fig. 8e–g). Taken together, we demonstrate that NAT10 maintains

proper spindle assembly by acetylating Eg5 during mitosis. Loss of NAT10 function leads to mitotic catastrophe through attenuating Eg5 acetylation at K771 (Fig. 8h).

DISCUSSION

Eg5 inhibition blocks bipolar spindle formation and successful mitosis completion [19, 56], whereas overexpression of Eg5 results in aneuploidy and genetic instability [57, 58]. Therefore, the optimal expression level of Eg5 is critical for maintaining proper mitosis. Here we demonstrate that NAT10 regulates Eg5 level through its acetyltransferase activity. Disruption of NAT10-mediated Eg5 acetylation leads to mitotic catastrophe.

It was reported that RNF20/40 complex promotes the mono-ubiquitination at K745 to protect Eg5 from degradation during mitosis [21], while APC/C reduces the stability of Eg5 in the cancer cells with centrosome amplifications [22]. However, the mechanisms of Eg5 stability regulation are largely unknown. In the present study, we demonstrate that the stability of Eg5 is regulated by NAT10. Further, the acetyltransferase activity of NAT10 is required for its function in stabilizing Eg5. We further identified K771 as the major acetylation site catalyzed by NAT10. The substitution of K771 by arginine (K771R) reduces the protein stability of Eg5. Thus, we have identified K771 as an acetylation site controlling the stability of Eg5. Further, Eg5 K771R mutation dramatically increased its poly-ubiquitination level (Supplementary Fig. 5a, b), indicating that acetylation at K771 regulates Eg5 stability through inhibiting the poly-ubiquitination of Eg5. Additionally, the mono-ubiquitination of Eg5 at K745 was not effectively affected by K771-Ac (Supplementary Fig. 5c), further confirming that K771-Ac controls Eg5 stabilization through poly-ubiquitination. By searching the database, we found that Eg5 might be ubiquitinated at multiple sites (https://www.phosphosite.org/). However, the detailed mechanism about the K771 acetylation-mediated poly-ubiquitination of Eg5 needs to be elucidated.

Since Eg5 loading in the centrosome is essential for the poleward movement of centrosome, we therefore determined if NAT10 affects the centrosome loading of Eg5. We show that the immunofluorescence staining signals of Eg5 in the centrosome are reduced when NAT10 was depleted. Thereafter, we found that NAT10 regulates Eg5 stability, thus the decreased Eg5 level in the centrosomes might be, at least partially, due to reduced total level of Eg5. It is known that the phosphorylation of Eg5 Thr926 is essential for the centrosome loading of Eg5 [15]. To determine if K771 acetylation affects the centrosome loading of Eg5, we evaluated the effect of K771 acetylation on the Thr926 phosphorylation. We show that Flag-Eg5 K771R (loss of acetylation) reduces the phosphorylation level of Thr926 and Eg5 K771Q (hyper-acetylation mimic) increases the Thr926 phosphorylation level, confirming that K771 acetylation also affects the centrosome loading by regulating Thr926 phosphorylation. However, how Eg5 K771-Ac regulates the phosphorylation of Eg5-Thr926 needs further study.

To further verify that Eg5-K771 acetylation acts in the centrosome, we generated the K771-Ac specific antibody. Immunofluorescence staining with Eg5-K771-Ac antibody shows that Eg5 K771-Ac specifically localizes in the centrosomes during mitosis, providing evidence for Eg5 K771-Ac functioning in the centrosome. Given that pEg5-Thr926 controls the centrosome movement, Eg5-K771-Ac might affect the centrosome movement. Since Flag-Eg5 is not able to be acetylated in the NAT10 KO cells, ectopic Flag-Eg5 should not rescue the *NAT10* KO-retarded centrosome movement. Indeed, the *NAT10* KO retarded centrosome movement was only rescued by the hyper-acetylation mimic Flag-Eg5 K771Q but not by Flag-Eg5 or Flag-Eg5 K771R. Additionally, the monopolar spindle formation and mitotic catastrophe were rescued only by Flag-Eg5-K771Q but not Flag-Eg5 and Flag-Eg5 K771R. These findings demonstrate that K771-Ac controls the motor function of Eg5.

It has been known that the acetylation at K146 of Eg5 enhances the binding of Eg5 with MTs and to slowdown the poleward movement [18, 19]. In addition, Acetylation at K890 inhibits the ATP hydrolysis capability of Eg5 and blocks spindle assembly. K890 of Eg5 is de-acetylated by HDAC to promote mitosis [20]. In the present study, we found that acetylation of K771 is required for the poleward movement. Our findings expand the understanding of the functional regulation of Eg5 by acetylation, and the de-acetylation of Eg5 K771 is worth of further study.

The Eg5 inhibitors have already been under clinical trials in the treatment of hematopoietic malignancies, bladder cancer and advanced solid tumors treatment as they trigger mitotic catastrophe [8, 59, 60]. Therefore, regulators functioning in the mitotic catastrophe may provide more choices in the tumor therapy. In this study, we demonstrate that NAT10 is a novel acetyltransferase of Eg5. NAT10 acetylates Eg5 at K771 to control the protein stabilization and the motor function of Eg5. Targeting NAT10 induces mitotic catastrophe through decreasing Eg5 level and inhibiting Eg5 motor function. We thus provide a novel mechanism for better understanding the effect of targeting NAT10 in tumor therapy. Additionally, small molecules blocking Eg5 K771-Ac would also possess anti-tumor potential.

In summary, depletion of NAT10 or loss of its acetyltransferase activity results in mitotic catastrophe. NAT10 acetylates Eg5 K771 to stabilize Eg5 and control the Eg5-mediated centrosome movement. Thus, our findings expand the understanding of the acetylation-mediated regulation of expression level and the motor function of Eg5. Our data suggest that targeting the NAT10-mediated Eg5 K771 acetylation is a potential strategy for anti-tumor therapy.

DATA AVAILABILITY

The datasets used and/or analyzed during the current study are available from the corresponding author on reasonable request.

REFERENCES

1. Gordon DJ, Resio B, Pellman D. Causes and consequences of aneuploidy in cancer. Nat Rev Genet. 2012;13:189–203.
2. Ricke RM, van Deursen JM. Aneuploidy in health, disease, and aging. J Cell Biol. 2013;201:11–21.
3. Vitale I, Galluzzi L, Castedo M, Kroemer G. Mitotic catastrophe: a mechanism for avoiding genomic instability. Nat Rev Mol Cell Biol. 2011;12:385–92.
4. Galluzzi L, Vitale I, Aaronson SA, Abrams JM, Adam D, Agostinis P, et al. Molecular mechanisms of cell death: recommendations of the Nomenclature Committee on Cell Death 2018. Cell Death Differ. 2018;25:486–541.
5. Hanahan D, Weinberg RA. Hallmarks of cancer: the next generation. Cell. 2011;144:646–74.
6. Jordan MA, Wilson L. Microtubules as a target for anticancer drugs. Nat Rev Cancer. 2004;4:253–65.
7. Huszar D, Theoclitou ME, Skolnik J, Herbst R. Kinesin motor proteins as targets for cancer therapy. Cancer Metastasis Rev. 2009;28:197–208.
8. Rello-Varona S, Vitale I, Kepp O, Senovilla L, Jemaa M, Metivier D, et al. Preferential killing of tetraploid tumor cells by targeting the mitotic kinesin Eg5. Cell Cycle. 2009;8:1030–5.
9. Mayer TU, Kapoor TM, Haggarty SJ, King RW, Schreiber SL, Mitchison TJ. Small molecule inhibitor of mitotic spindle bipolarity identified in a phenotype-based screen. Science 1999;286:971–4.
10. Tunquist BJ, Woessner RD, Walker DH. Mcl-1 stability determines mitotic cell fate of human multiple myeloma tumor cells treated with the kinesin spindle protein inhibitor ARRY-520. Mol Cancer Ther. 2010;9:2046–56.
11. Marcus AI, Peters U, Thomas SL, Garrett S, Zelnak A, Kapoor TM, et al. Mitotic kinesin inhibitors induce mitotic arrest and cell death in Taxol-resistant and -sensitive cancer cells. J Biol Chem. 2005;280:11569–77.
12. Nakai R, Iida S, Takahashi T, Tsujita T, Okamoto S, Takada C, et al. K858, a novel inhibitor of mitotic kinesin Eg5 and antitumor agent, induces cell death in cancer cells. Cancer Res. 2009;69:3901–9.
13. Miglarese MR, Carlson RO. Development of new cancer therapeutic agents targeting mitosis. Expert Opin Investig Drugs. 2006;15:1411–25.

14. Hernandez-Garcia S, San-Segundo L, Gonzalez-Mendez L, Corchete LA, Misiewicz-Krzeminska I, Martin-Sanchez M, et al. The kinesin spindle protein inhibitor filanesib enhances the activity of pomalidomide and dexamethasone in multiple myeloma. Haematologica. 2017;102:2113–24.
15. Blangy A, Lane HA, d'Herin P, Harper M, Kress M, Nigg EA. Phosphorylation by p34cdc2 regulates spindle association of human Eg5, a kinesin-related motor essential for bipolar spindle formation in vivo. Cell. 1995;83:1159–69.
16. Sawin KE, Mitchison TJ. Mutations in the kinesin-like protein Eg5 disrupting localization to the mitotic spindle. Proc Natl Acad Sci USA. 1995;92:4289–93.
17. Avunie-Masala R, Movshovich N, Nissenkorn Y, Gerson-Gurwitz A, Fridman V, Koivomagi M, et al. Phospho-regulation of kinesin-5 during anaphase spindle elongation. J Cell Sci. 2011;124:873–8.
18. Choudhary C, Kumar C, Gnad F, Nielsen ML, Rehman M, Walther TC, et al. Lysine acetylation targets protein complexes and co-regulates major cellular functions. Science. 2009;325:834–40.
19. Muretta JM, Reddy BJN, Scarabelli G, Thompson AF, Jariwala S, Major J, et al. A posttranslational modification of the mitotic kinesin Eg5 that enhances its mechanochemical coupling and alters its mitotic function. Proc Natl Acad Sci USA. 2018;115:E1779–E88.
20. Nalawansha DA, Gomes ID, Wambua MK, Pflum MKH. HDAC inhibitor-induced mitotic arrest is mediated by Eg5/Klf11 acetylation. Cell Chem Biol. 2017;24:481–92. e5.
21. Duan Y, Huo D, Gao J, Wu H, Ye Z, Liu Z, et al. Ubiquitin ligase RNF20/40 facilitates spindle assembly and promotes breast carcinogenesis through stabilizing motor protein Eg5. Nat Commun. 2016;7:12648.
22. Drosopoulos K, Tang C, Chao WC, Linardopoulos S. APC/C is an essential regulator of centrosome clustering. Nat Commun. 2014;5:3686.
23. Kong R, Zhang L, Hu L, Peng Q, Han W, Du X, et al. hALP, a novel transcriptional U three protein (t-UTP), activates RNA polymerase I transcription by binding and acetylating the upstream binding factor (UBF). J Biol Chem. 2011; 286:7139–48.
24. Ito S, Horikawa S, Suzuki T, Kawauchi H, Tanaka Y, Suzuki T, et al. Human NAT10 is an ATP-dependent RNA acetyltransferase responsible for N4-acetylcytidine formation in 18 S ribosomal RNA (rRNA). J Biol Chem. 2014;289:35724–30.
25. Cai S, Liu X, Zhang C, Xing B, Du X. Autoacetylation of NAT10 is critical for its function in rRNA transcription activation. Biochem Biophys Res Commun. 2017;483:624–9.
26. Sharma S, Langhendries JL, Watzinger P, Kotter P, Entian KD, Lafontaine DL. Yeast Kre33 and human NAT10 are conserved 18S rRNA cytosine acetyltransferases that modify tRNAs assisted by the adaptor Tan1/THUMPD1. Nucleic Acids Res. 2015;43:2242–58.
27. Dominissini D, Rechavi GN. N(4)-acetylation of cytidine in mRNA by NAT10 regulates stability and translation. Cell. 2018;175:1725–7.
28. Thomas JM, Bryson KM, Meier JL. Nucleotide resolution sequencing of N4-acetylcytidine in RNA. Methods Enzymol. 2019;621:31–51.
29. Arango D, Sturgill D, Alhusaini N, Dillman AA, Sweet TJ, Hanson G, et al. Acetylation of cytidine in mRNA promotes translation efficiency. Cell. 2018;175:1872–86. e24.
30. Liu X, Tan Y, Zhang C, Zhang Y, Zhang L, Ren P, et al. NAT10 regulates p53 activation through acetylating p53 at K120 and ubiquitinating Mdm2. EMBO Rep. 2016;17:349–66.
31. Zhang L, Li DQ. MORC2 regulates DNA damage response through a PARP1-dependent pathway. Nucleic Acids Res. 2019;47:8502–20.
32. Liu HY, Liu YY, Yang F, Zhang L, Zhang FL, Hu X, et al. Acetylation of MORC2 by NAT10 regulates cell-cycle checkpoint control and resistance to DNA-damaging chemotherapy and radiotherapy in breast cancer. Nucleic Acids Res. 2020;48:3638–56.
33. Liu X, Cai S, Zhang C, Liu Z, Luo J, Xing B, et al. Deacetylation of NAT10 by Sirt1 promotes the transition from rRNA biogenesis to autophagy upon energy stress. Nucleic Acids Res. 2018;46:9601–16.
34. Larrieu D, Britton S, Demir M, Rodriguez R, Jackson SP. Chemical inhibition of NAT10 corrects defects of laminopathic cells. Science. 2014;344:527–32.
35. Wu J, Zhu H, Wu J, Chen W, Guan X. Inhibition of N-acetyltransferase 10 using remodelin attenuates doxorubicin resistance by reversing the epithelial-mesenchymal transition in breast cancer. Am J Transl Res. 2018;10:256–64.
36. Tsai K, Jaguva Vasudevan AA, Martinez Campos C, Emery A, Swanstrom R, Cullen BR. Acetylation of cytidine residues boosts HIV-1 gene expression by increasing viral RNA stability. Cell Host Microbe. 2020;28:306–12. e6.
37. Balmus G, Larrieu D, Barros AC, Collins C, Abrudan M, Demir M, et al. Targeting of NAT10 enhances healthspan in a mouse model of human accelerated aging syndrome. Nat Commun. 2018;9:1700.
38. Larrieu D, Vire E, Robson S, Breusegem SY, Kouzarides T, Jackson SP. Inhibition of the acetyltransferase NAT10 normalizes progeric and aging cells by rebalancing the Transportin-1 nuclear import pathway. Sci Signal. 2018;11:eaar5401.
39. Liu Z, Liu X, Li Y, Ren P, Zhang C, Wang L, et al. miR-6716-5p promotes metastasis of colorectal cancer through downregulating NAT10 expression. Cancer Manag Res. 2019;11:5317–32.
40. Tschida BR, Temiz NA, Kuka TP, Lee LA, Riordan JD, Tierrablanca CA, et al. Sleeping beauty insertional mutagenesis in mice identifies drivers of steatosis-associated hepatic tumors. Cancer Res. 2017;77:6576–88.
41. Oh TI, Lee YM, Lim BO, Lim JH. Inhibition of NAT10 suppresses melanogenesis and melanoma growth by attenuating microphthalmia-associated transcription factor (MITF) expression. Int J Mol Sci. 2017;18:1924–35.
42. Wachtler F, Popp W, Schwarzacher HG. Structural changes in nucleoli during inhibition of protein- and RNA-biosynthesis. Cell Tissue Res. 1987; 247:583–9.
43. Orsolic I, Jurada D, Pullen N, Oren M, Eliopoulos AG, Volarevic S. The relationship between the nucleolus and cancer: Current evidence and emerging paradigms. Semin Cancer Biol. 2016;37-38:36–50.
44. Scheer U, Thiry M, Goessens G. Structure, function and assembly of the nucleolus. Trends Cell Biol. 1993;3:236–41.
45. Chi YH, Haller K, Peloponese JM Jr., Jeang KT. Histone acetyltransferase hALP and nuclear membrane protein hsSUN1 function in de-condensation of mitotic chromosomes. J Biol Chem. 2007;282:27447–58.
46. Shen Q, Zheng X, McNutt MA, Guang L, Sun Y, Wang J, et al. NAT10, a nucleolar protein, localizes to the midbody and regulates cytokinesis and acetylation of microtubules. Exp Cell Res. 2009;315:1653–67.
47. Cho YC, Park JE, Park BC, Kim JH, Jeong DG, Park SG, et al. Cell cycle-dependent Cdc25C phosphatase determines cell survival by regulating apoptosis signal-regulating kinase 1. Cell Death Differ. 2015;22:1605–17.
48. van Ree JH, Nam HJ, Jeganathan KB, Kanakkanthara A, van Deursen JM. Pten regulates spindle pole movement through Dlg1-mediated recruitment of Eg5 to centrosomes. Nat Cell Biol. 2016;18:814–21.
49. Crosio C, Fimia GM, Loury R, Kimura M, Okano Y, Zhou H, et al. Mitotic phosphorylation of histone H3: spatio-temporal regulation by mammalian Aurora kinases. Mol Cell Biol. 2002;22:874–85.
50. Koller E, Propp S, Murray H, Lima W, Bhat B, Prakash TP, et al. Competition for RISC binding predicts in vitro potency of siRNA. Nucleic Acids Res. 2006;34:4467–76.
51. Bertran MT, Sdelci S, Regue L, Avruch J, Caelles C, Roig J. Nek9 is a Plk1-activated kinase that controls early centrosome separation through Nek6/7 and Eg5. EMBO J. 2011;30:2634–47.
52. Zou SW, Zhang JC, Zhang XD, Miao SY, Zong SD, Sheng Q, et al. Expression and localization of VCX/Y proteins and their possible involvement in regulation of ribosome assembly during spermatogenesis. Cell Res. 2003;13:171–7.
53. Mann BJ, Wadsworth P Kinesin-5 regulation and function in mitosis. Trends Cell Biol. 2019;29:66–79.
54. Liu M, Ran J, Zhou J. Non-canonical functions of the mitotic kinesin Eg5. Thorac Cancer. 2018;9:904–10.
55. Hata S, Pastor Peidro A, Panic M, Liu P, Atorino E, Funaya C, et al. The balance between KIFC3 and EG5 tetrameric kinesins controls the onset of mitotic spindle assembly. Nat Cell Biol. 2019;21:1138–51.
56. Eguren M, Alvarez-Fernandez M, Garcia F, Lopez-Contreras AJ, Fujimitsu K, Yaguchi H, et al. A synthetic lethal interaction between APC/C and topoisomerase poisons uncovered by proteomic screens. Cell Rep. 2014;6:670–83.
57. Castillo A, Morse HC 3rd, Godfrey VL, Naeem R, Justice MJ. Overexpression of Eg5 causes genomic instability and tumor formation in mice. Cancer Res. 2007;67:10138–47.
58. Liu M, Wang X, Yang Y, Li D, Ren H, Zhu Q, et al. Ectopic expression of the microtubule-dependent motor protein Eg5 promotes pancreatic tumourigenesis. J Pathol. 2010;221:221–8.
59. Khoury HJ, Garcia-Manero G, Borthakur G, Kadia T, Foudray MC, Arellano M, et al. A phase 1 dose-escalation study of ARRY-520, a kinesin spindle protein inhibitor, in patients with advanced myeloid leukemias. Cancer. 2012;118:3556–64.
60. Carter BZ, Mak DH, Woessner R, Gross S, Schober WD, Estrov Z, et al. Inhibition of KSP by ARRY-520 induces cell cycle block and cell death via the mitochondrial pathway in AML cells. Leukemia. 2009;23:1755–62.

ACKNOWLEDGEMENTS

We thank Dr. Qihua He for assistance with confocal microscopy, Dr. Xiajuan Zou for assistance in the mass spectrometric analysis. We thank Prof. Bo Zhang for providing us the anti-NAT10 antibody and Prof. Chenghao Xuan for providing us the GFP-RNF20 and GFP-RNF40 plasmids.

AUTHOR CONTRIBUTIONS

JZ designed and performed experiments, analyzed the data and wrote the manuscript. YT performed the experiments and analyzed the data. XL helped with

the mass spectrometry analysis. CZ helped with cell culture and purchased the reagents. KS helped with protein purification. YJ helped with live-cell imaging. JL provided experiment help and revised the manuscript. LL designed and supervised the study. XD designed and acquired the funding for the study, analyzed the data and revised the manuscript.

FUNDING

This work was supported by the grants from the National Natural Science Foundation of China (Grant No. 82173024 and 81874143 to XD), the Beijing Natural Science Foundation (Grant No.7212061 to XD) and the National Natural Science Foundation of China (Grant No. 81802305 to XL).

COMPETING INTERESTS

The authors declare no competing interests.

ETHICS STATEMENT

This study was approved by the Ethics Committee of the Peking University Health Science Center.

ADDITIONAL INFORMATION

Supplementary information The online version contains supplementary material available at https://doi.org/10.1038/s41418-021-00899-5.

Correspondence and requests for materials should be addressed to Li Li or Xiaojuan Du.